Scalar nonlinear continuum damage models for ceramic matrix composites with significant in plane ply anisotropy

Craig Przybyla, Antoine Débarre, Jean-François Maire, Emmanuel Baranger, Frédéric Laurin

SCALER NONLINEAR CONTINUUM DAMAGE MODELS FOR CERAMIC MATRIX COMPOSITES WITH SIGNIFICANT IN PLANE PLY ANISOTROPY

Craig Przybyla[a], Antoine Débarre[b], Jean-François Maire[b], Emmanuel Baranger[c], Frédéric Laurin[c]

a: Air Force Research Laboratory, Wright-Patterson AFB, OH, USA – craig.przybyla@us.af.mil
b: l'Office National d'Études et de Recherches Aérospatiales, Châtillon, France
c: Laboratoire de Mécanique Paris-Saclay, Gif-sur-Yvette, France

Abstract: *Continuous fiber reinforced ceramic matrix composites (CMCs) are increasingly being employed in safety critical applications and the need the need for damage models to support the design, certification and sustainment has increased. In this work, we propose a simple but robust formulation for a 2D continuum damage model derived via a thermodynamics-based approach called openDM. Specifically, we consider a model with two scalar damage parameters that account for damage as a result of matrix cracking in the ply in both the fiber and transverse directions. The applicability of this model is considered for both a balanced 2D woven based SiC fiber reinforced composite and a 2D unidirectional ply based SiC fiber reinforced composite with predominately SiC matrices. While the response of the 2D woven composite was captured well with the two parameter model, the more anisotropic unidirectional ply based CMC was more difficult to capture unless a hybrid [0,90] ply was assumed in the model.*

Keywords: Continuum damage model; ceramic matrix composites; anisotropic damage response

1. Introduction

As the use of continuous fiber reinforced ceramic matrix composites (CMCs) has rapidly accelerated, particularly in aero-propulsion, the need for damage models to support the design, certification and sustainment of safety critical CMC components has increased. One CMC variant with continuous SiC fibers embedded into a predominately SiC matrix has been of particular interest for components in the hot section of gas turbine engines. Recently, CFM started selling their new LEAP® engine with SiC/SiC CMC shrouds (1). Despite these successes, the requirements for insertion of these types of materials in critical applications such as gas-turbine engines for aerospace require extensive testing for design, certification and sustainment. Progressive damage modelling tools that can better inform designs, provide accurate life assessments for certification and address sustainment issues after systems have been fielded have the potential to greatly reduce the required amount of testing, reduce conservatism in design, and provide sustainment engineers with the ability to perform performance prognosis in the presence of defects or in service damage.

Typically SiC/SiC CMCs are designed with a weak fiber coating or interphase of pyrolytic carbon or boron nitride that promotes a toughened response (2,3). The architecture of the fiber reinforcement can be stacks of 2D plys, 3D woven preforms or unidirectional laminate based layups (4). They are typically processed either using a mixture of chemical vapour infiltration/deposition (CVI/CVD) and polymer infiltration and pyrolysis or densified using a melt infiltration (MI) process with silicon melted into a carbon preform. Several studies have characterized the mechanical behavior. At the microscale, the cracks appear to initially form

near the weak interphase or defects and grow dependent on local microstructural conditions (5). In dense MI based systems, the cracks have been observed to initiated near the interphase and coalesce into larger matrix cracking with increasingly large loads (6,7). At larger scales, damage in the laminate based MI SiC/SiC CMCs appears in bands (8,9). In the more porous PIP derived matrices with 2D woven plies, the damage appears to depend on the weave architecture with the major cracks forming at specific cross over points in the tows (10). These observations indicate that there is a strong influence of microstructure on initiation and propagation and that damage propagation is very dependent on the direction of loading.

Continuum damage modelling (CDM) approaches that estimate an effective or average damage state over a given volume have been frequently employed to model the mechanical response of CMCs. Chaboche et. al. (11) introduced a CDM model for brittle materials that employed a tensorial damage variable that accounts for damage deactivation and irreversible strains. Later Chaboche and Maire (12) expanded on the approach include deactivation due to closure in compression. In this model, Chaboche and Maire employed both scalar damage variables corresponding with microcracks oriented by the orientation of the fibre reinforcement and a second rank damage tensor that evolves with the maximum principal strain directions. Marcin et. al. (13) employed the same framework developed earlier by Chaboche and Maire, but used five scalar damage variables to account damage in the direction of the primary reinforcement, transverse to the direction of the primary reinforcement, in the ±45° directions and in the out of plane direction. Baranger (14) and Friderikos and Baranger (15) showed that reduced order models (such as the scaler model by Marcin et. al. (13)) can be as accurate as complex models with tensorial damage variables for a wide range of loading cases.

In this work we follow the approach of Marcin et. al. (13) to develop a simple two parameter model to capture the in plane effects effects of the primary damage modes observed in 2D ply based layups including woven and unidirectional laminates but limit our analysis to two scale damage variables for the in plane response.

2. Methods

2.1 Model Formulation

In this approach the continuum damage formulation is based on the Helmholtz free energy to derive a thermodynamically consistent relationship for the deformation response. A simple 2D damage model can be formulated such that the Helmholtz free energy is defined according to

$$\psi = \frac{1}{2\rho}\left(\varepsilon^* : \tilde{\mathbf{C}} : \varepsilon^*\right) \tag{1}$$

where

$$\boldsymbol{\varepsilon}^* = \boldsymbol{\varepsilon} - \boldsymbol{\varepsilon}^{th} \tag{2}$$

The compliance is related to the stiffness according to

$$\tilde{\mathbf{C}} = \left(\tilde{\mathbf{S}}\right)^{-1} \tag{3}$$

The effective compliance is defined as

$$\tilde{\mathbf{S}} = \mathbf{S}^0 + \Delta\mathbf{S}^m \tag{4}$$

such that $\Delta\mathbf{S}^m$ is the variation of the initial compliance tensor $\mathbf{S}^0$ as a result of the matrix damage.

For a thin plate we can assume either plane stress or plane strain boundary conditions. The resulting compliance tensor can be expressed as

$$\mathbf{S}^0 = \begin{bmatrix} \frac{1}{E_{11}} & \frac{-\nu_{12}}{E_{11}} & 0 \\ \frac{-\nu_{21}}{E_{22}} & \frac{1}{E_{22}} & 0 \\ 0 & 0 & \frac{1}{G_{12}} \end{bmatrix} \tag{5}$$

with a total of four independent elastic constants including the elastic moduli in the two orthogonal directions E_{11} and E_{22}, the in-plane Poisson ratio ν_{12} and the in-plane shear modulus G_{12}. Note that the Poisson ratio ν_{12} is related to ν_{21} according to $\nu_{12}/E_{11} = \nu_{21}/E_{22}$. The elastic stiffness is defined as $\mathbf{C}^0$ and ρ is the material density. It follows then that the behavior law is

$$\boldsymbol{\sigma} = \rho\frac{\partial\psi}{\partial\boldsymbol{\varepsilon}} = \tilde{\mathbf{C}}\colon\boldsymbol{\varepsilon}^* \tag{6}$$

The strain is determined according to

$$\boldsymbol{\varepsilon} = \tilde{\mathbf{S}}\colon\boldsymbol{\sigma} + \boldsymbol{\varepsilon}^{th} \tag{7}$$

The total strain tensor is defined as $\boldsymbol{\varepsilon}$ and the thermal strain tensor $\boldsymbol{\varepsilon}^{th}$ is defined such that

$$\boldsymbol{\varepsilon}^{th} = \boldsymbol{\alpha}(T - T^0) \tag{8}$$

where $\boldsymbol{\alpha}$ is the symmetric thermal expansion tensor, T is the current or test temperature and T^0 is the reference temperature. We employ two scalar damage variables (d_1^m, d_2^m) to account for matrix damage in the 0° and 90° loading directions. The superscript m indicates damage in the matrix and not in the fibers. The change in compliance based on damage $\Delta\mathbf{S}^m$ can be simplified to as

$$\Delta\mathbf{S}^m = \sum_{i=1}^{2} d_i^m\mathbf{H}_i^m \tag{9}$$

where $\mathbf{H}_i^m$ is the fourth-order damage-effect tensor. Here we assume a simple deactivation index η_i^m as defined previously. As the behavior in the transverse direction (relative to the loading axis) remains linear, the form of the fourth order damage-effect tensor is expressed as

$$\mathbf{H}_1^m = \begin{pmatrix} \eta_1^m S_{11}^0 & 0 & 0 \\ 0 & 0 & 0 \\ 0 & 0 & h_{66}^1 S_{66}^0 \end{pmatrix} \tag{10}$$

and

$$\mathbf{H}_2^m = \begin{pmatrix} 0 & 0 & 0 \\ 0 & \eta_2^m S_{22}^0 & 0 \\ 0 & 0 & h_{66}^2 S_{66}^0 \end{pmatrix} \tag{11}$$

The model parameter h_{66}^1 and h_{66}^2 correspond to the effect of the stress acting parallel to the plane of the crack and parallel to the crack front, respectively.

The deactivation index η_i^m is defined such that

$$\eta_i^m = h(\sigma_i) \tag{12}$$

where h is the Heaviside step function. This indicates that the cracks are closed under compressive stresses. The driving forces y_i^m associated with the two scalar damage variables d_i^m are defined as a function of the positive part of the total strain tensor such that:

$$\begin{cases} y_1^m = \frac{1}{2}(E_{11}\langle\varepsilon_1^*\rangle_+^2 + b_1 G_{12}(\varepsilon_6^*)^2) \\ y_2^m = \frac{1}{2}(E_{22}\langle\varepsilon_2^*\rangle_+^2 + b_2 G_{12}(\varepsilon_6^*)^2) \end{cases} \tag{13}$$

where $\langle . \rangle_+$ are the Macaulay Brackets. The model parameter b_1 define the coupling between tension and in plane shear. We then define

$$\begin{cases} y_1^{max} = \max\limits_{0<\tau\leq t}(y_1^m(\tau)) \\ y_2^{max} = \max\limits_{0<\tau\leq t}(y_2^m(\tau)) \end{cases} \tag{14}$$

Finally, we define an exponential form of the scalar function that accounts for saturation effects such that

$$g_{s(i)}^{max}(y) = \frac{\left\langle \sqrt{y_{(i)}^{max}} - \sqrt{y_{0(i)}^m} \right\rangle_+}{\sqrt{y_{c(i)}^m}} \tag{15}$$

and the damage variables d_i can be calculated as

$$d_i = d_{c(i)}^m \left[1 - \exp\left\{-\left(g_{s(i)}^{max}\right)^{p_i^m}\right\}\right] \quad \text{for } i \in \{1,2\} \tag{16}$$

where the model parameter $d_{c(i)}^m$ describes the saturation damage parameter, $y_{0(i)}^m$ is the damage threshold, $y_{c(i)}^m$ describes the influence of the damage rate, and p_i^m accounts for the curve shape. The parameters for the 2D damage model are summarized in Table 1.

2.2 Model Implementation

Here we employ generalized non-linear composite laminate theory to solve the material model for thin composites with 2D plys oriented at various angles relative to the sample reference frame. Following the Kirshoff-Love theory, we assume that the total mesoscopic strain relative to the global reference frame is linear in the thickness of the laminate such that

$$\boldsymbol{\varepsilon} = \boldsymbol{\varepsilon}^0 + z\boldsymbol{\kappa}^0 \tag{17}$$

where $\boldsymbol{\varepsilon}^0$ and $\boldsymbol{\kappa}^0$ are the membrane strain and the curvature of the laminate and z is the perpendicular distance to the middle plane of the laminate. It is assumed here that the deformed shape remains normal to the middle-plane during loading and that the out-of-plane shear strains are negligible. The governing equilibrium equations for the composite layup are

$$\mathbf{N} + \mathbf{N}^g + \mathbf{N}^{th} = \mathbf{A}\colon\boldsymbol{\varepsilon}^0 + \mathbf{B}\colon\boldsymbol{\kappa}^0 \tag{18}$$

and

$$\mathbf{M} + \mathbf{M}^{g} + \mathbf{M}^{th} = \mathbf{B}\colon \boldsymbol{\varepsilon}^{0} + \mathbf{D}\colon \boldsymbol{\kappa}^{0} \tag{19}$$

where $\mathbf{N}$ and $\mathbf{M}$ are the Loads and bending moments applied to the laminate. The superscript g denotes the loads and moments associated with the non-linear strains, and the superscript th indicates those associated with the thermal strains. The nonlinear strains in the ply coordinate system can be calculated such that

$$(\boldsymbol{\varepsilon}^{\boldsymbol{g}})^{p} = \left[\mathbf{I} - \mathbf{S}(T_0)^{p}\colon \tilde{\mathbf{C}}(T, \boldsymbol{d})^{p}\right]\colon \left[\boldsymbol{\varepsilon}^{\boldsymbol{p}} - \left(\boldsymbol{\varepsilon}^{th}\right)^{\boldsymbol{p}}\right] \tag{20}$$

and the thermal strains were defined previously. The matrices $[\mathbf{A}]$, $[\mathbf{B}]$, and $[\mathbf{D}]$ in equations (18) and ((19) are called the extensional stiffness, the coupling stiffness and the bending stiffness, respectively, and are defined elsewhere (16). Schematics explaining the resultant forces $\mathbf{N}$ and resultant moments $\mathbf{M}$ are given in Figure 1.

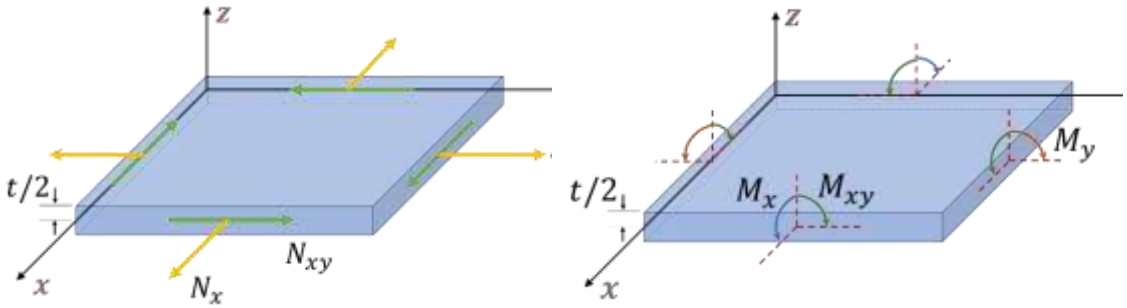

(a) (b)

Figure 1 Schematic showing the definitions of the (a) force and (b) moment resultants

3. Results and Discussion

3.1 2D woven SiC/SiC composite

The first material that was considered was a 2D continuous woven SiC fiber CMC with a predominately SiC matrix. The weave was balanced with equal fiber volume fraction in the 0° and 90° directions with no off angle plies in the layup. Data were available for tensile tests in both the 0° and 45° degree direction relative to the direction of the warp tows. The experimental data and model results are both given in Figure 2.

Several iterations were employed by adjusting the model parameters for calibration. Specifically, this calibration was performed using a specific procedure such that

1. Estimate elastic parameters based on constituents and rule of mixtures (E_{11}^{0}, E_{22}^{0}, ν_{12}^{0}, G_{12}^{0}, α_i, T_o)
2. Calibrate Elastic Parameters for 0°tests (E_{11}^{0}, E_{22}^{0})
3. Calibrate Elastic Parameters for 45°tests (G_{12}^{0})
4. Calibrate damage parameters for 0°tests ($y_{0(i)}^{m}$, $y_{c(i)}^{m}$, p_i^{m}, $d_{c(i)}^{m}$)
5. Calibrate damage parameters for 45°tests (h_{66}^{i}, b_i)
6. Iterate parameters to find best fit for 0°and 45°tests

The calibrated parameters are given in Table 1.

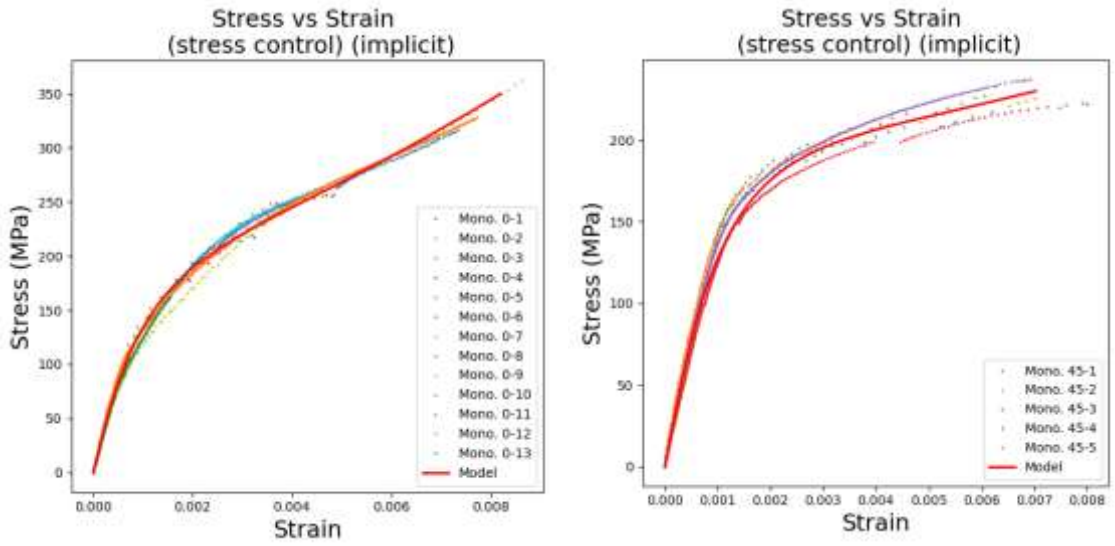

(a) (b)

Figure 2: Experimental stress versus strain response with the openDM model predicitons for 2D woven SiC/SiC (a) oriented 0° relative to the loading direction, (b) oriented 45° relative to the loading direction.

Table 1: Calibration parameters for 2D woven SiC/SiC CMC

Elasticity	$\boldsymbol{E_{11}^0 = E_{22}^0} = 180GPa$ $\boldsymbol{\nu_{12}^0} = 0.1$ $\boldsymbol{G_{12}^0} = 68GPa$	Young Modulus Poisson ratio Shear modulus
Thermal behavior	$\boldsymbol{\alpha_1 = \alpha_2} = 3.7x10^{-6}$ 1/℃ $\boldsymbol{T_o} = 20$℃	Thermal expansion Reference Temperature
Damage effects	$\boldsymbol{h_{66}^1 = h_{66}^2} = 1.35$	"Shear" Damage Effect
Thermodynamic forces	$\boldsymbol{b_1 = b_2} = 0.3$	Traction / Shear Coupling
Damage Kinetics	$\boldsymbol{y_{0(1)}^m = y_{0(2)}^m} = 0.003$ $\boldsymbol{y_{c(1)}^m = y_{c(2)}^m} = 2.2$ $\boldsymbol{p_1^m = p_2^m} = 1.3$ $\boldsymbol{d_{c(1)}^m = d_{c(2)}^m} = 3.8$	Damage Thresholds Damage Evolution Celerity Damage Evolution Exponents Damage Saturations

3.2 Unidirectional Laminate based SiC/SiC CMC

The second material considered was a laminate based material with unidirectional SiC fibers embedded in a SiC matrix produced via the MI process. In all cases the material considered here was laid using an eight ply $[0,90]_{4s}$ layup. To accommodate the significant anisotropy between the 0° and 90° loading it was helpful to model each ply as a hybrid [0,90] ply stack instead of individual plies. The experimental data relative to the calibrated model are shown in Figure 3. The calibrated model parameters are in Table 2

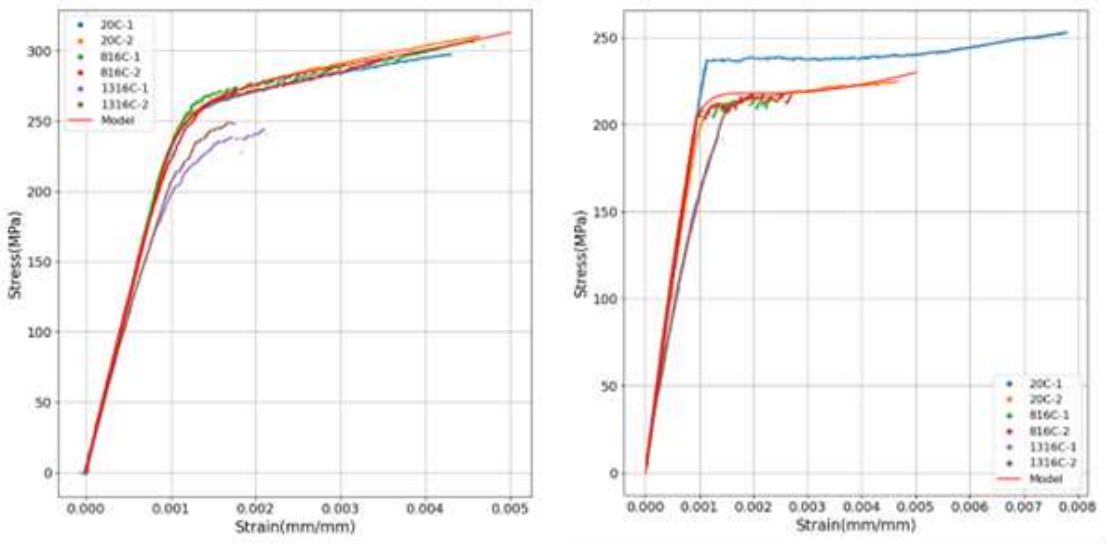

(c) (d)

Figure 3: Experimental stress versus strain response with the openDM model predicitons for (a) the GE SiC/SiC CMC oriented 0° relative to the loading direction and (b) the GE SiC/SiC CMC oriented 45° relative to the loading direction.

Table 2: Calibration parameters for Laminate based

Elasticity	$E_{11}^0 = E_{22}^0 = 290GPa$ $\nu_{12}^0 = 0.17$ $G_{12}^0 = 95.36GPa$	Young Modulus Poisson ratio Shear modulus
Thermal behavior	$\alpha_1 = \alpha_2 = 8.6x10^{-7}\ 1/℃$ $T_o = 20℃$	Thermal expansion Reference Temperature
Damage effects	$h_{66}^1 = h_{66}^2 = 0.8$	"Shear" Damage Effect
Thermodynamic forces	$b_1 = b_2 = 2.4$	Traction / Shear Coupling
Damage Kinetics	$y_{0(1)}^m = y_{0(2)}^m = 0.13$ $y_{c(1)}^m = y_{c(2)}^m = 6.3$ $p_1^m = p_2^m = 1.16$ $d_{c(1)}^m = d_{c(2)}^m = 6.3$	Damage Thresholds Damage Evolution Celerity Damage Evolution Exponents Damage Saturations

4. Conclusion

A simple 2D two parameter scaler continuum damage model was introduced to model the stress strain response in 2D CMC layups. The model is able to match the behavior well when the response of the plies is similar in the 0° and 90° directions such as is the case with a CMC with balance 2D woven plies. Unidirectional ply based CMCs can also be modeled using the simple two scale damage parameter model as stacks of coupled [0/90] degree plies. In this manner, it the same calibration proceeded can be employed with the coupled coupled [0/90] degree plies that was employed for the 2D balanced woven based CMC. However, it is likely that to model the highly anisotropic response of a single ply in a unidirectional ply based layup a more complex damage model will be required.

References

1. Steibel J. Ceramic matrix xomposites taking flight at GE Aviation. American Ceramic Society Bulletin. 2019; 98: 30-33.
2. DiCarlo JA, Yun HM, Morscher GN, Bhatt RT. Handbook ofCeramic Composites. In Bansal NP, editor..: KLUWER ACADEMIC PUBLISHERS; 2005. p. 77-98.
3. Corman GS, Luthra KL. Handbook ofCeramic Composites. In Bansal NP, editor..: KLUWER ACADEMIC PUBLISHERS; 2005. p. 99-115.
4. DiCarlo JA. Ceramic matrix Composites: materials, Modeling and Technology. In Bansal NP, Lamon J, editors..: Wiley; 2015. p. 217-235.
5. Swaminathan B, McCarthy NR, Almansour AS, Sevener K, Pollock TM, Kiser JD, et al. Microscale characterization of damage accumulation in CMCs. Journal of the European Ceramic Society. 2021; 41: 3082-3093.
6. Tracy J, Daly S, Sevener K. Multiscale damage characterization in continuous fiber ceramic matrix composites using digital image correlation. Journal of Materials Science. 2015/08/; 50: 5286-99.
7. Sevener KM, Tracy JM, Chen Z, Kiser JD, Daly S. Crack opening behavior in ceramic matrix composites. Journal of the American Ceramic Society. 2017; 100: 4734-4747.
8. Whitlow T, Jones E, Przybyla C. In-situ damage monitoring of a SiC/SiC ceramic matrix composite using acoustic emission and digital image correlation. Composite Structures. 2016; 158: 245-251.
9. Whitlow T, Pitz J, Pierce J, Hawkins S, Samuel A, Kollins K, et al. Thermal-mechanical behavior of a SiC/SiC CMC subjected to laser heating. Composite Structures. 2019; 210: 179-188.
10. Rossol MN, Rajan VP, Zok FW. Effects of weave architecture on mechanical response of 2D ceramic composites. Composites Part A: Applied Science and Manufacturing. 2015; 74: 141-152.
11. Chaboche JL, Lesne PM, Maire JF. On the constitutive damage modelling of composite systems. In ; 1995; Boulder. p. 223-226.
12. Chaboche JL, Maire JF. A new micromechanics based CDM model and its application to CMC's. Aerospace Science and Technology. 2002; 6: 131-145.
13. Marcin L, Maire JF, Carrere N, Martin E. Development of a Macroscopic Damage Model for Woven Ceramic Matrix Composites. International Journal of Damage Mechanics. 2011/08/; 20: 939-57.
14. Baranger E. Building of a reduced constitutive law for ceramic matrix composites. International Journal of Damage Mechanics. 2013; 22: 1222-1238.
15. Friderikos O, Baranger E. Automatic building of a numerical simplified constitutive law for Ceramic Matrix Composites using Singular Value Decomposition. International Journal of Damage Mechanics. 2016/05/; 25: 506-37.
16. Berthelot JM. Mécanique des Matériaux et Structures Composites: Institut Supérieur des Matériaux et Mécaniques Avancés; 2010.
17. Talreja R. Continuum modelling of damage in ceramic matrix composites. Mechanics of Materials. 1991; 12: 165-180.

18. Corman GS, Luthra KL. Melt infiltrated ceramic composites (HIPERCOMP®) for gas trubine engine applications. Tech. rep. United States Deptartment of Energy; 2006 January.
19. Corman GS, Luthra KL. Handbook of ceramic composites. In Bansal N, editor..: Springer; 2010.
20. Whitlow T, Jones E, Przybyla C. In-situ damage monitoring of a SiC/SiC ceramic matrix composite using acoustic emission and digital image correlation. Composite Structures. 2016; 158: 245-51.
21. Zawada LP, Carson LE, Przybyla C. MICROSTRUCTURAL AND MECHANICAL CHARACTERIZATION OF 2-D AND 3-D SiC/SiNC CERAMIC MATRIX COMPOSITES. 2018/02/;: 148p -.
22. Evans AG, Zok FW. The physics and mechanics of fibre-reinforced brittle matrix composites. Journal of Materials Science. 1994; 29: 3857-96.
23. Rossol MN, Fast T, Marshall DB, Cox BN, Zok FW. Characterizing in-plane geometrical variability in textile ceramic composites. Journal of the American Ceramic Society. 2015; 98: 205-213.
24. Ben Ramdane C. Étude et Modélisation du Comportemement Mécanique de CMC Oxyde/Oxyde. Ph.D. dissertation. , L'Université de Bordeaux; 2014 June.
25. Marcin L. Modélisation du Comportement, de L'Endommagement et de la Rupture de Matériaux Composites Á Renforts Tissés pour le Dimensionnement Robuste de Structures. Ph.D. dissertation. , L'Université Bordeaux 1; 2010.

